XL CILAMCE
IBERO-LATIN AMERICAN CONGRESS ON COMPUTATIONAL METHODS IN ENGINEERING
NOVEMBER 11-14, 2019
Praiamar Natal Hotel & Convention Natal, RN-BRAZIL

NUMERICAL INTEGRATION OF GREEN'S FUNCTIONS FOR LAYERED MEDIA: A CASE STUDY

Cavalcante I.
Labaki J.
i209496@dac.unicamp.br
labaki@fem.unicamp.br
School of Mechanical Engineering, University of Campinas
Rua Mendeleyev 200, 13083-860, São Paulo, Campinas, Brazil

Abstract. Classical Green's functions for transversely isotropic media are typically expressed in terms of improper integrals containing a number of singularities and a decaying tail that oscillates indefinitely. Currently, there are no known numerical methods capable of dealing precisely with both characteristics of these integrands simultaneously. In this work, Green's functions for layered media are presented in terms of an exact stiffness matrix scheme, in which a stiffness matrix for the medium is assembled from the stiffness matrices of each layer. The integrand in such cases is characterized by an infinite number of singularities, corresponding to the propagation and reflection waves in the medium. The oscillatory-decaying tail presents more than one frequency of oscillation, which makes them difficult to integrate by classical extrapolation methods. This work presents strategies with which to evaluate such integrals numerically. We have shown that the singularities can be located within the integration interval at points that correspond to physical wavenumbers of each layer, which are then integrated through a appropriate contour deformation paths. For the oscillatory-decaying part, we use a combination of strategies. The first is to use Fast Fourier Transforms to break down the oscillation into its component frequencies. The fundamental frequency is used to yield a sequence of partial sums, from which the integral can be obtained by extrapolation though the ϵ-algorithm. As a case study, the scheme is used to evaluate the displacement of layered, transversely isotropic soil medium under time-harmonic external excitations. The results are compared with classical adaptive quadrature integration schemes.

Keywords: Numerical integration, Green's function, Countor deformation paths, Extrapolation

1 Introduction

Dynamic soil-foundation interaction models often require the derivation of Green functions corresponding to surface or buried loads and the characteristics of the material medium that represent the problem. Classical Green's functions for transversely isotropic media are typically expressed in terms of improper integrals with respect to the upper limit of integration containing a number of singularities and a decaying tail that oscillates indefinitely. The numerical evaluation of such integrals is remarkably difficult to obtain; there are currently no numerical methods that is able to handle both characteristics of these integrands accurately.

The Green's functions for a case of the time-harmonic response of an elastic transversely isotropic layered media subjected to an axisymmetric load on its surface are consider in this work. The layered media is described by the exact stiffness matrix scheme [1], in which a stiffness matrix for the medium is assembled from the stiffness matrices of each layer. The solution, displacements of the layered system, can be approached through the Hankel transform [1, 2], which must be numerically integrated to obtain the corresponding response in the physical domain. The normalization of the integration variable proposed by Rajapakse and Wang [2], causes the singularities to fall within a predictable region allowing the integrand to be divided into two distinct regions, each requiring a specialized integration technique. However, the evaluation of these integrals is difficult and has a high computational cost [3, 4] because its integrands in such cases are characterized by an infinite number of singularities, induced by different wave modes corresponding to body, propagation, reflection and interface waves in the medium. In layered media, the oscillatory-decaying tail presents more than one frequency of oscillation, which makes them difficult to integrate by classical extrapolation methods.

This work presents strategies with which to evaluate such integrals numerically. We have shown that the singularities can be located within the integration interval at points that correspond to physical wavenumbers of each layer and these have a direct connection with mathematical brach cuts in the integration path [5]. This technique is used to locate the singularities in an example case of layered medium, which are then integrated through a complex-plane contour approach around the integration variable. This approach enables bypassing the treatment of singularities by simply deforming the contour of integration through a complex half-plane [6–11].

For the oscillatory-decaying part, we use a combination of strategies. The first is to use fast Fourier transforms (FFT) to break down the oscillation into its component frequencies [12]. This step enables the extraction of the fundamental frequency that characterizes the periodicity of the signal. From that frequency, one can create a sequence of partial sums so that the integral can be obtained by extrapolation though the ϵ-algorithm [13] according to a numerical scheme initially proposed by Cavalcante and Labaki [14]. This technique is shown to work even when the integrand is given by transcendental functions [14], such as the case when Green's functions are obtained with the aid of Hankel transforms.

As a case study, the scheme is used to evaluate the displacement of a layered, transversely isotropic soil medium under time-harmonic external excitations. The results are compared with classical adaptive quadrature integration schemes with smoothing out the singular region by introducing a small damping factor to the constitutive parameters of the medium.

2 Formulation

Consider a case of the time-harmonic displacement response of an elastic transversely isotropic layered medium subjected to an axisymmetric load, the motion equation of which is described in cylindrical coordinates by the displacements $u_i(r, z)$ in the r and z directions respectively. The cylindrical coordinates system is placed so that the z axis is orthogonal to the material's plane of isotropy, and the load is applied on the $x - y$ plane and centered at the origin. Rajapakse and Wang [2] derived a solution for these displacement fields through Hankel transforms, which are given by:

$$u_i = \delta^2 \int_0^\infty u_i^* \zeta d\zeta, \quad i = r, z, \tag{1}$$

where $\zeta = \lambda'/\delta$, in which λ' is the wave number (Hankel space variable) and δ is a normalized frequency of excitation. The displacements kernels (u_i^*) are given by:

$$u_r^* = a_1 A e^{-\delta\xi_1 z} + a_1 B e^{\delta\xi_1 z} + a_2 C e^{-\delta\xi_2 z} + a_2 D e^{\delta\xi_2 z}, \tag{2}$$

$$u_z^* = -(a_7 A e^{-\delta\xi_1 z} - a_7 B e^{\delta\xi_1 z} + a_8 C e^{-\delta\xi_2 z} - a_8 D e^{\delta\xi_2 z}). \tag{3}$$

The coefficients A, B, C and D are arbitrary functions that can be determined from the boundary and continuity conditions of a given problem. The other parameters in Eqs. (1) to (3) are described in the Appendix.

Displacement and stress fields for the case of an N-layered half-space (Fig. 1) have been derived by Labaki et al. [4] from a general expression presented earlier by Rajapakse and Wang [2]. The radial and vertical displacements $u_i^*(z_n)$, $i = r, z$, $n = 1, N+1$ of the layer interfaces due to radial and vertical loads at arbitrary layers is given in the Hankel transformed domain by

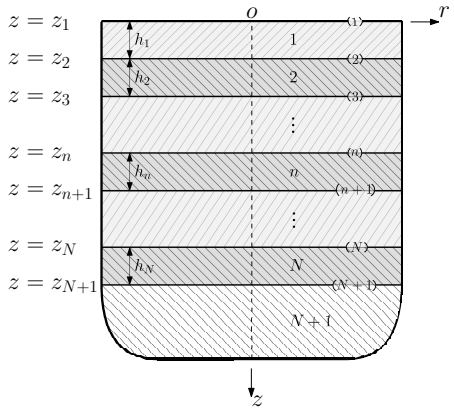

Figure 1. Geometry of layered half-space.

$$\wp^* = K u^*, \tag{4}$$

in which

$$\wp^* = \left\langle \begin{array}{cccccc} \wp_r^{*1} & \wp_z^{*1} & \dots & \wp_r^{*(N+1)} & \wp_z^{*(N+1)} \end{array} \right\rangle^T, \tag{5}$$

$$u^* = \left\langle \begin{array}{cccccc} u_r^*(r, z_1) & u_z^*(r, z_1) & \dots & u_r^*(r, z_{N+1}) & u_z^*(r, z_{N+1}) \end{array} \right\rangle^T. \tag{6}$$

where $\wp^*$ is the vector of external loads applied at the layer interfaces. A vertical disc load p_0 distributed on an annular area with outer and inner radii s_2 and s_1 can be represented in the Hankel transformed domain by $\wp_{z_n}^{*n} = 1/\zeta[s_2 J_1(\zeta s_2) - s_1 J_1(\zeta s_1)]p_0$, $n = 1, N+1$. The global stiffness matrix of the medium is assembled with the stiffness matrices of each layer.

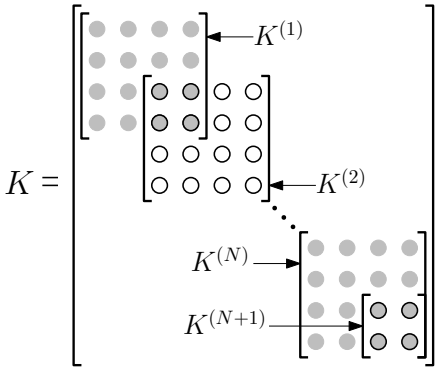

Figure 2. Global stiffness matrix assembly scheme.

The sections $K^{(n)}$ in Fig. 2 are the stiffness matrices of layer i, given by $K^{(n)} = F^{(n)}(G(n))^{-1}$, where

$$G^{(n)} = \begin{bmatrix} a_1 e_{1,n}^{-1} & a_1 e_{1,n}^{+1} & a_2 e_{2,n}^{-1} & a_2 e_{2,n}^{+1} \\ -a_7 e_{1,n}^{-1} & a_7 e_{1,n}^{+1} & -a_8 e_{2,n}^{-1} & -a_8 e_{2,n}^{+1} \\ a_1 e_{1,n+1}^{-1} & a_1 e_{1,n+1}^{+1} & a_2 e_{2,n+1}^{-1} & a_2 e_{2,n+1}^{+1} \\ -a_7 e_{1,n+1}^{-1} & a_7 e_{1,n+1}^{+1} & -a_8 e_{2,n+1}^{-1} & a_8 e_{2,n+1}^{+1} \end{bmatrix} \tag{7}$$

and

$$\frac{F^{(n)}}{c_{44}^{(n)}} = \begin{bmatrix} b_{51} e_{1,n}^{-1} & -b_{51} e_{1,n}^{+1} & b_{52} e_{2,n}^{-1} & -b_{52} e_{2,n}^{+1} \\ -b_{21} e_{1,n}^{-1} & -b_{21} e_{1,n}^{+1} & -b_{22} e_{2,n}^{-1} & -b_{22} e_{2,n}^{+1} \\ -b_{51} e_{1,n+1}^{-1} & b_{51} e_{1,n+1}^{+1} & -b_{52} e_{2,n+1}^{-1} & b_{52} e_{2,n+1}^{+1} \\ b_{21} e_{1,n+1}^{-1} & b_{21} e_{1,n+1}^{+1} & b_{22} e_{2,n+1}^{-1} & b_{22} e_{2,n+1}^{+1} \end{bmatrix} \tag{8}$$

for $n = 1, N$, and

$$G^{(N+1)} = \begin{bmatrix} a_1 e_{1,N+1}^{-1} & a_2 e_{2,N+1}^{-1} \\ -a_7 e_{1,N+1}^{-1} & -a_8 e_{2,N+1}^{-1} \end{bmatrix} \tag{9}$$

and

$$\frac{F^{(N+1)}}{c_{44}^{(n)}} = \begin{bmatrix} b_{51} e_{1,N+1}^{-1} & b_{52} e_{2,N+1}^{-1} \\ -b_{21} e_{1,N+1}^{-1} & -b_{22} e_{2,N+1}^{-1} \end{bmatrix} \tag{10}$$

for $n = N + 1$ (half-space). In Eqs. (7) to (10), $e_{i,j}^{\pm 1} = e^{\pm \delta^{(n)} \xi_i^{(n)} z_j}$, $i = 1, 2$, $j = 1, N + 1$. All other variables in Eqs. (4) to (10) are presented in the Appendix.

3 Integration method

The previous section presented the exact stiffness method to obtain the Green's function for the layered medium for axisymmetric loads. The normalization of the integration variable proposed by Rajapakse and Wang [2], $\zeta = \lambda/\delta$, causes all singularities to fall within a predictable region, which allows the integrand to be divided into two distinct regions, each one to be solved by an appropriate method of integration. The integration regions are defined as: Region I ($0 \leq \zeta \leq \zeta^{'}$), which is characterized by the presence of singularities, and Region II ($\zeta^{'} \leq \zeta \leq \infty$), where the integrand oscillates and decays in amplitude indefinitely. The value of $\zeta^{'}$ is selected in this work to ensure that Region II of the integrand is free of singularities.

3.1 Region I: Contour deformation path

For an arbitrary layered system, it is impracticable to determine all singularities in the integration path, since these points vary in position and quantity according to almost all system parameters. The integration path may be properly deformed at the top of the ζ-complex half-plane to avoid the singularities.

The requirement for the successful application of the deformed path of integration in a particular multilayer problem is the careful sketch of the integrand with singularities in the relevant region of the complex plane. Cavalcante and Labaki [5] showed that the singularities arising in the stiffness matrix of each layer correspond to the pressure and shear waves expected in the Green's functions that describe a homogeneous half-space. These wavenumbers are, respectively,

$$k_P = \pm\sqrt{1/\beta}, \tag{11}$$

$$k_S = \pm 1. \tag{12}$$

For a multilayered media it is observed an additional singularity given by

$$k_I = \pm \frac{\sqrt{-1+\alpha+\kappa}}{\sqrt{-1+\alpha\beta+2\kappa-\kappa^2}}. \tag{13}$$

In addition, it is expected the existence of simple poles corresponding to Rayleigh, Stoneley and Love wave numbers. These singularities occur due to zeros of the denominators in the inversion of the global stiffness matrix (Fig. 2). Unlike the Rayleigh wave, which will always exists in media possessing a free surface, the Stoneley and Love waves may or may not exist depending on the material parameters and system configuration. The complete discussion on the conditions for the existence of poles associated with the Stoneley and Love waves can be found in Barnett et al. [15], Barnett [16], and Kuznetsov [17].

The singularity associated with the Rayleigh waves for layered media is very close to the Rayleigh waves for a homogeneous half-space case. These wavenumber are $k_R = k$, such that

$$[2(1-\kappa)k^2 - \gamma k^2 + \alpha](1-k^2) - \alpha\xi_1\xi_2 = 0. \tag{14}$$

The parameters involved in Eqs. (11) to (14) are a function of the normalized elastic constants of the material and are shown in the Appendix.

The contour deformation path approach has been explored for this class of problems by Guzina and Pak [6], Golubovic et al. [7], Chatterjee et al. [8], Chatterjee et al. [9], Michalski and Mosig [10] and Durbhakula et al. [11] and enables the integrals corresponding to an elastic solution to be evaluated, that is, the case in which the layers and the half-space have no damping characteristics. Although the form of the modified contour of integration is not critical, its height in the imaginary axis is limited by the exponential growth of the Bessel function in the real axis [10, 11]. In this work, the semi-elliptical contour (SE) is chosen as modified integration path (Fig. 3).

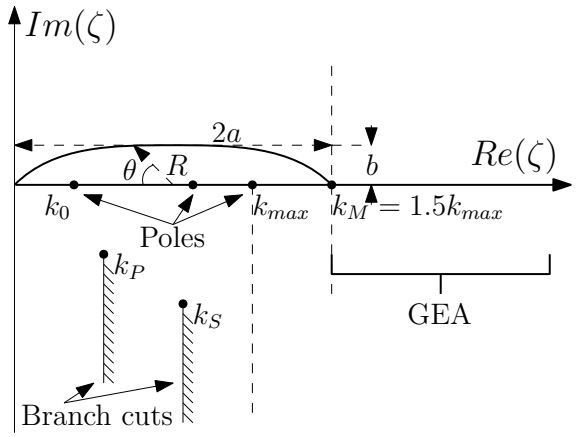

Figure 3. Semi-elliptical modified integration path.

The semi-major axis of the ellipse is $a = 1/2k_M$. The choice of the semi-minor axes of the ellipse is given as follows:

$$b = \begin{cases} k_0 \times \min\left(1, \frac{k_0^{-1}}{2\pi f_\rho}\right), & \text{para} \quad 2\pi f_\rho > |z_n| \\ k_0, & \text{para} \quad 2\pi f_\rho \leq |z_n|, \end{cases} \tag{15}$$

where k_{max} is adopted as the Rayleigh wavenumber, k_0 is the smaller singularity between k_P, k_S and k_I, and f_ρ is the fundamental frequency determined in the approach of the next section.

3.2 Region II: Partition-extrapolation method

This region is characterized by the presence of an irregular oscillatory behavior because integrands of the Green's functions involve multiplications of Bessel functions (arbitrary number of oscillatory

frequencies) arising from the solution of the linear system (Eq. (4)). This linear system contains Bessel functions in the variables defined in the Appendix and in the load described in the transformed Hankel domain in Eq. (5), as well as exponential terms expressed in Eqs. (7) to (10).

The integral in Region II will be evaluated using the fast Fourier transforms (FFT) to decompose the oscillation periods and extract the fundamental frequency (f_ρ) that characterizes the periodicity of the signal. That frequency is used to create a sequence of partial sums based on the partition of Sidi [18] to be extrapolated with the aid of the ϵ-algorithm [13]. This numerical scheme has been initially proposed by Cavalcante and Labaki [14].

The integration interval is divided into a number of subintervals, each of which is a partial sum in the ϵ-algorithm's extrapolation scheme. The subintervals are defined by

$$\zeta_n = b_1 + \frac{\pi n}{f_\rho}, \quad n \geq 0. \tag{16}$$

Figure 3 illustrates the region where the generalization of the ϵ-algorithm based on the FFT (GEA) will be applied. In this works, b_1 is defined as the first zero of the integrand greater than k_M.

3.3 Numerical results and discussion

In this section, the implementation of the layered media model by the global stiffness matrix method is used to describe a case of time-harmonic response of a multilayered transversely isotropic soil with an axisymmetric load on its surface. This study considers a soil constituted by a layer in contact with a half-space (Fig. 4).

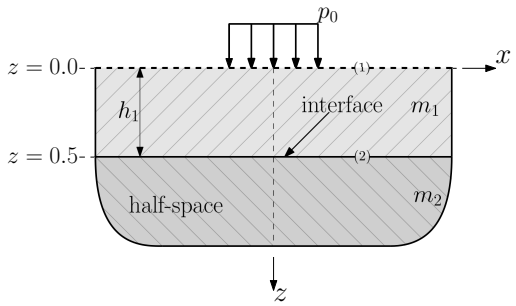

Figure 4. Geometry of the multilayered system.

The material and thickness of the layers are shown in Table 1. The layers and the half-space are transversely isotropic media with Poisson's coefficient ν and specific mass ρ.

Table 1. Multilayered media setting used ($c'_{ij} = c_{ij}/c_{44}$).

Layer	$\mathbf{h_i}$	**Material**	$\mathbf{c'_{11}}$	$\mathbf{c'_{12}}$	$\mathbf{c'_{13}}$	$\mathbf{c'_{33}}$	ρ	ν
1	0.5	m_1	3.0000	1.0000	1.0000	3.0000	1.0000	0.25
half-space	∞	m_2	4.2200	2.0300	1.6200	4.5300	0.9167	0.32

The results from the present integration scheme are compared with those of a classical Gauss adaptive quadrature (AGQ). In order for the AGQ algorithm to be able to handle the singularities in the integrand, a small damping is introduced into the formulation according to the elastic-viscoelastic correspondence principle [19]:

$$c_{ij} = c^*_{ij}(1 + i\eta). \tag{17}$$

In Eq. (17) c^*_{ij} are real elastic constants that define the transversely isotropic material and c_{ij} are their complex counterparts. A hysteretic damping model is considered, in which the damping factor η is a constant [20]. Figure 5 shows the real and imaginary parts of the dynamic vertical displacement $u_z(\omega)$

of this layered medium obtained with the present implementation. The results show real and imaginary parts of $u_z(\omega)$ at the surface of the soil ($z = 0$) and at the layer interface ($z = 0.5$). The results are compared with those obtained with the AGQ.

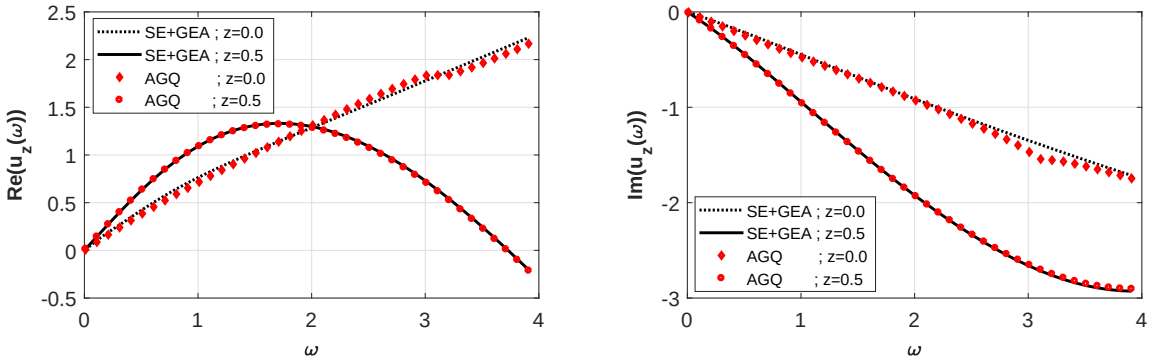

Figure 5. Real and imaginary parts of the vertical displacement $u_z(\omega)$ by present scheme (SE+GEA) and AGQ for different excitation frequency (ω).

The vertical displacement $u_z(\omega)$ for different thicknesses (h_1) of the layer is shown in Fig. 6 with excitation frequency $\omega = 1$. Uniformly distributed loads are considered with fixed values $p_0 = 1$, $s_2 = 1$ and $s_1 = 0$.

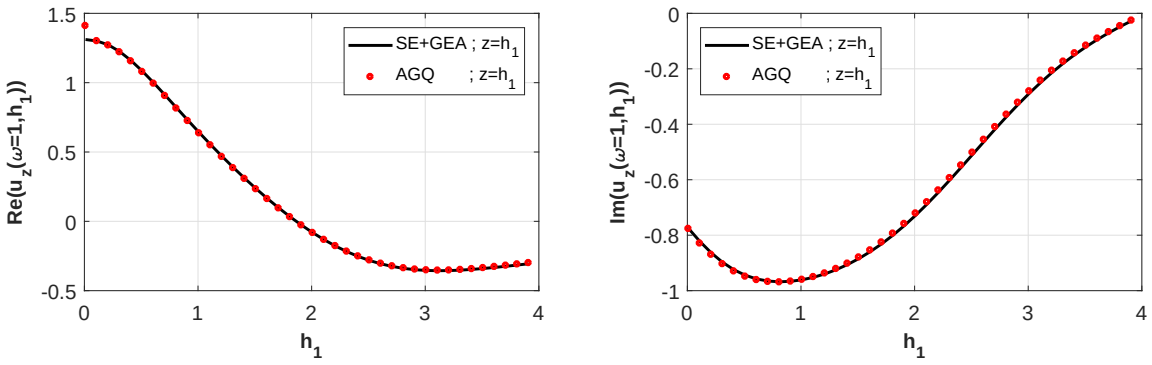

Figure 6. Real and imaginary parts of the vertical displacement $u_z(\omega = 1)$ by present scheme (SE+GEA) and AGQ for different thicknesses (h_1).

Figure 7 shows the influence of the inner radius s_1 of the loaded area in $u_z(\omega)$ considering the fixed values $p_0 = 1$, $s_2 = 4$, $\omega = 1$, $h = 0.5$.

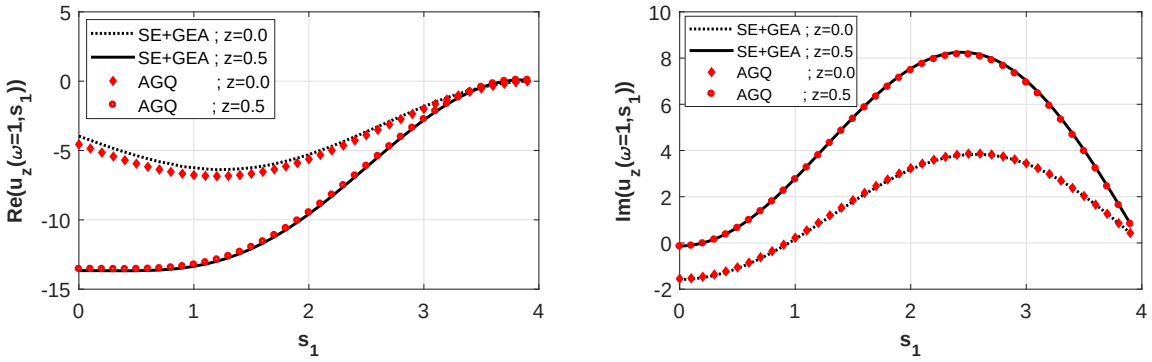

Figure 7. Real and imaginary parts of the vertical displacement $u_z(\omega = 1)$ by present scheme (SE+GEA) and AGQ for different inner radii (s_1).

For the evaluation of the singular region by the AGQ, the integration interval is divided into smaller regions beginning and ending at the points of singularities corresponding to the branch cuts k_S, k_P, k_I and the poles k_R. The second region is evaluated with the direct application of AGQ [21].

4 Conclusion

This work proposed a numerical integration scheme to deal with improper integrals with respect to the upper limit of integration of functions with an oscillatory decaying behavior, containing an infinite number of singularities. This scheme was used to evaluate the displacement of a layered, transversely isotropic soil medium under time-harmonic external excitations. The results obtained by the numerical scheme formed by the contour deformation path method for the singular interval together to the generalization of the ϵ-algorithm based on the FFT for the oscillatory-decaying part showed that this approach produces accurate results for different sets of constitutive parameters.

5 Appendix

This appendix lists the parameters appearing in Eqs. (1) to (10), for $i = 1, 2$,

$$b_{2i} = [\alpha\delta^2\xi_i^2 - (\kappa - 1)\delta^2\zeta^2\vartheta_i]J_0(\delta\zeta r). \tag{18}$$

$$\frac{a_7}{\delta\xi_1} = \frac{a_8}{\delta\xi_2} = J_0(\delta\zeta r). \tag{19}$$

$$\frac{a_i}{\vartheta_i} = \frac{b_{5i}}{(1+\vartheta_i)\delta^2\xi_i} = -\delta^2\xi_i J_1(\delta\zeta r). \tag{20}$$

In Eqs. (18) to (20), J_m is the Bessel function of the first kind and m^{th} order and

$$\vartheta_{1,2} = \frac{\alpha\xi_{1,2}^2 - \zeta^2 + 1}{\kappa\zeta^2}. \tag{21}$$

$$\xi_{1,2} = \frac{1}{\sqrt{2\alpha}}(\gamma\zeta^2 - 1 - \alpha \pm \sqrt{\Phi})^{\frac{1}{2}}. \tag{22}$$

$$\Phi = (\gamma\zeta^2 - 1 - \alpha)^2 - 4\alpha(\beta\zeta^4 - \beta\zeta^2 - \zeta^2 + 1). \tag{23}$$

$$\alpha = \frac{c_{33}}{c_{44}}, \quad \beta = \frac{c_{11}}{c_{44}}, \quad \kappa = \frac{c_{13} + c_{44}}{c_{44}}, \quad \delta^2 = \frac{\rho\omega^2}{c_{44}} \quad \text{and} \quad \gamma = 1 + \alpha\beta - \kappa^2. \tag{24}$$

where δ is a normalized frequency of excitation, ω is the frequency of excitation, and c_{ij} are elastic contants of the transversely isotropic material.

Permission

The authors are the only responsible for the printed material included in this paper.

Acknowledgements

The research leading to this article has been funded in party by the São Paulo Research Foundation - Fapesp, through grand 2017/01450-0. The support of Capes, CNPq, and Faepex-Unicamp is also gratefully acknowledged.

References

[1] Wang, Y. & Rajapakse, R. K. N. D., 1994. An exact stiffness method for elastodynamics of a layered orthotropic half-plane. *Journal of Applied Mechanics*, vol. 61, n. 2, pp. 339–348.

[2] Rajapakse, R. K. N. D. & Wang, Y., 1993. Green's functions for transversely isotropic elastic half space. *Journal of Engineering Mechanics-asce*, vol. 119, n. 9, pp. 1724–1746.

[3] Barros, P. L. A., 2006. Impedances of rigid cylindrical foundations embedded in transversely isotropic soils. *International Journal for Numerical and Analytical Methods in Geomechanics*, vol. 30, n. 7, pp. 683–702.

[4] Labaki, J., Mesquita, E., & Rajapakse, R. K. N. D., 2014. Vertical vibrations of an elastic foundation with arbitrary embedment within a transversely isotropic, layered soil. *Cmes-computer Modeling in Engineering and Sciences*, vol. 103, n. 5, pp. 281–313.

[5] Cavalcante, I. & Labaki, J., 2019a. Correlation between physical wavenumbers and singularities in the integrand of green's functions for layered media. In *MECSOL 2019*.

[6] Guzina, B. & Pak, R., 2001. On the analysis of wave motions in a multi-layered solid. *The Quarterly Journal of Mechanics and Applied Mathematics*, vol. 54, n. 1, pp. 13–37.

[7] Golubovic, R., Polimeridis, A. G., & Mosig, J. R., 2012. Efficient algorithms for computing sommerfeld integral tails. *IEEE Transactions on Antennas and Propagation*, vol. 60, n. 5, pp. 2409–2417.

[8] Chatterjee, D., Rao, S. M., & Kluskens, M. S., 2013. Improved evaluation of sommerfeld integrals for microstrip antenna problems. *2013 International Symposium on Electromagnetic Theory*, pp. 981–984.

[9] Chatterjee, D., Rao, S., & Kluskens, M., 2016. Some new techniques for evaluating sommerfeld integrals for microstrip antenna analysis. In *2016 URSI International Symposium on Electromagnetic Theory (EMTS)*, pp. 335–337. IEEE.

[10] Michalski, K. A. & Mosig, J. R., 2016. Efficient computation of sommerfeld integral tails – methods and algorithms. *Journal of Electromagnetic Waves and Applications*, vol. 30, n. 3, pp. 281–317.

[11] Durbhakula, K. C., Hassan, A. M., Chatterjee, D., & Kluskens, M. S., 2017. Evaluation of sommerfeld integrals using contour deformation paths for nano and microstrip antenna applications. In *2017 IEEE Applied Electromagnetics Conference (AEMC)*.

[12] Telgarsky, R., 2013. Dominant frequency extraction. *CoRR*, vol. abs/1306.0103.

[13] Wynn, P., 1956. On a device for computing the and m (s n) transformation. *Mathematical Tables and Other Aids to Computation*, vol. 10, n. 54, pp. 91.

[14] Cavalcante, I. & Labaki, J., 2019b. An fft-based generalization of the e-algorithm for the integration of oscillatory-decaying functions with multiple frequencies. In *DINAME 2019*.

[15] Barnett, D. M., Lothe, J., Gavazza, S. S., & Musgrave, M. J. P., 1985. Considerations of the existence of interfacial (stoneley) waves in bonded anisotropic elastic half-spaces. *Proceedings of the royal society of London, series A : mathematical and physical sciences*, vol. 402, n. 1822, pp. 153–166.

[16] Barnett, D. M., 2000. Bulk, surface, and interfacial waves in anisotropic linear elastic solids. *International Journal of Solids and Structures*, vol. 37, pp. 45–54.

[17] Kuznetsov, S. V., 2006. Love waves in layered anisotropic media. *Journal of Applied Mathematics and Mechanics*, vol. 70, n. 1, pp. 116–127.

[18] Sidi, A., 1982. The numerical evaluation of very oscillatory infinite integrals by extrapolation. *Mathematics of Computation*, vol. 38, n. 158, pp. 517–529.

[19] Christensen, R. M., 1982. *Theory of Viscoelasticity*. Elsevier.

[20] Gaul, L., 1999. The influence of damping on waves and vibrations. *Mechanical Systems and Signal Processing*, vol. 13, n. 1, pp. 1–30.

[21] Piessens, R., de Doncker-Kapenga, E., Überhuber, C. W., & Kahaner, D. K., 1983. *Quadpack: a subroutine package for automatic integration*, volume 1. Springer.